A micromechanical bridging law model for CFCCs

Konstantinos G. Dassios [a,*], Vassilis Kostopoulos [b], Marc Steen [c]

[a] *Foundation of Research and Technology Hellas, Institute of Chemical Engineering and High Temperature Chemical Processes,
Stadiou Street, Platani, Patras GR 26504, Achaia, Greece*
[b] *Department of Mechanical Engineering and Aeronautics, University of Patras, Rio GR 26500, Greece*
[c] *Institute for Energy, Joint Research Centre, European Commission, Westerduinweg 4, 1755 LE Petten, The Netherlands*

Abstract

In the present work, a methodology is presented for the assessment of bridging laws for continuous fibre-reinforced ceramic matrix composites based on material properties as well as micromechanics of fibre deformation and failure. A load–displacement model is initially formulated that utilizes weakest-link statistical concepts to analyse and relate the individual contributions of matrix, intact/bridging and failed/pull-out fibres during the composite fracture process. The total and individual contributions to the bridging law and crack growth resistance of the material are determined by identifying the non-elastic part of displacement as crack opening. The model is validated against the experimentally recorded load–displacement behaviour of a notched SiC-fibre-reinforced glass–ceramic matrix composite tested under monotonic tension. The output parameters of the converged regression procedure remain within a small scattering range from the corresponding mean values that compare favourably with known material properties. A parametric analysis of the effect of fibre volume fraction, Weibull modulus of fibres and interfacial shear stress in overall composite performance is presented in view of the ability of the model to serve as an a priori fracture prediction tool.
© 2006 Acta Materialia Inc. Published by Elsevier Ltd. All rights reserved.

Keywords: Ceramic matrix composites; Fiber reinforced composites; Fracture

1. Introduction

The brittle nature of ceramics has hindered the use of these materials in high-temperature applications with increased mechanical demands for many decades. The development, in the 1970s, of ceramic matrix composite (CMC) materials, consisting of a bulk ceramic phase, the matrix, reinforced by an embedded phase in the form of particulates, whiskers or fibres, unleashed the potential of these materials to equip a structure with a unique combination of properties to withstand simultaneous thermal and mechanical loading and pushed up the limits.

A specially designated class of CMCs that evolved during the 1990s, continuous fibre-reinforced ceramic matrix composites (CFCCs), with fibres of high length-to-diameter ratios, has become established as the strongest and toughest of all types of ceramic composites. CFCCs are used today as structural components in commercial and military aircraft and high-speed vehicles (e.g. braking systems, stabilizers), in aerospace applications (e.g. mechanical parts and thermal barriers for space shuttles, rocket nozzles), and in incinerators, heat exchangers and many other high-temperature applications. Among the admirable characteristics of CFCCs are their increased crack growth resistance and improved damage tolerance compared with monolithic ceramics, their notch insensitivity and their ability to effectively redistribute stresses around notches, voids and cracks. These prominent properties stem from the energy dissipation mechanisms activated during CFCC fracture that temper the fatal work of crack propagation at the crack front (crack process zone) by consuming a part of the externally applied energy. The two major energy dissipation mechanisms in CFCCs

are, in order of importance, matrix-crack bridging by intact fibres and pull-out of failed fibres. Both mechanisms are direct results of the interactions of a third phase in the composite, the interface region (interphase) between the matrix and the fibres, that, despite having a thickness of only a few nanometres, occupies a vast surface area in the composite and commands its macroscopical fracture behaviour. Externally applied stress is transmitted from the matrix to the bridging fibres through the interface zone while pull-out is a result of frictional sliding of the outer surface of failed fibres across the debonded interface.

The fracture behaviour of most contemporary CFCCs exhibits large-scale bridging (LSB), a phenomenon where the dimensions of the bridging zone formed by fibres bridging the separating crack flanks of a macro-crack during material fracture are large enough to be comparable to a characteristic specimen dimension (e.g. thickness). Under these conditions, conventional fracture mechanics parameters such as the crack growth resistance of the material are dependent on specimen dimension and configuration and cannot serve as material-intrinsic fracture descriptors [1,2].

An alternative approach proposed for the characterization of CFCC performance is the bridging law, a phenomenological correlation between the stresses acting on fibres within the bridging zone (bridging stresses) and the crack opening displacement (COD) [3]. Owing to its localized range of effect around the bridging zone, the law is believed capable of serving as a constitutive, material-intrinsic fracture descriptor that is independent of the overall composite dimensions or geometry. The determination of the bridging law for various composite systems has been the aim of several research efforts in the last decade. Different law forms have been indirectly evaluated using either micromechanical modelling approaches [4], energy-related approaches such as the J-integral [5,6], compliance-based techniques [7,8], weight function and stress intensity approaches [9] or weakest-link statistical considerations [10–12]. While the calculated bridging laws have, in general, succeeded in assessing the fracture behaviour of individual CFCCs used in the aforementioned studies, the current lack of confidence in CFCC applicability – especially with respect to the growing concern about high production costs – clearly demonstrates the necessity to comprehend the fundamentals of interactions between the composite phases using simple, straightforward methods. The biggest challenge in the composites world today is the linking of the physics and mechanics of micro- and nanoscale interactions to the overall composite performance.

In this study, a straightforward methodology is presented for the determination of bridging laws for composite materials exhibiting LSB and pull-out. The principle of the methodology relies on the deconvolution of the fracture behaviour of the composite into the individual contributions of the matrix, intact and failed fibres. Using simple Weibull statistical concepts to mathematically describe the fracture mechanism associated with each contribution and rational conditions to simulate the physics of their correlation during composite fracture, a model fracture law is initially developed that assesses the load–displacement behaviour of the composite. The bridging law is then obtained by a simple subtraction of the matrix contribution and the conversion of the load–displacement law to the stress-crack opening displacement form. The efficiency of the model relies on the simplicity of concepts used in its derivation, the minimal number of assumptions it invokes and its utilization of measurable parameters with explicit physical significance, such as the properties of the matrix, fibres and the interphase. The validity of the derived model is tested against the experimentally recorded fracture behaviour of a SiC-fibre-reinforced glass–ceramic matrix composite tested under quasi-static tensile loading. The ability of the model to predict, a priori, the fracture behaviour of a CFCC is discussed against the results of a parametric analysis of the role of material parameters. The model can securely predict the load–displacement behaviour of any kind of double-edge notch (DEN) configuration, while it can be extended for the prediction of the fracture behaviour of compact tension (CT) and single-edge-notch beam specimens.

2. Model formulation

The derivation of the model relies on the principle that the total load–displacement behaviour of a composite can be expressed as the sum of three terms corresponding to the individual contributions of the matrix, intact/bridging fibres and failed/pull-out fibres. For the formulation of the model, equal strain conditions are assumed to apply among the composite constituents, as in common displacement-controlled testing. The development of the model relies on the good understanding of the physics and mechanics of successive stages during CFCC fracture and the role of each of the composite's constituents (matrix, fibre and interphase) in these stages. The fracture procedure of a CFCC has been analysed in a previous study [13] and is summarized in the following.

2.1. Mechanical behaviour of a bridged crack

During the initial loading stages the composite deforms in a linear elastic manner until the first matrix micro-crack appears to trigger the formation of the bridging zone. Further loading leads to micro-cracks growing to fibre-bridged macro-cracks, while concurrent phenomena such as interface debonding and crack deflection at the interface take place. Depending on specimen configuration, the bridging zone may either span the whole width of the material, as, for example, in a DEN sample [13], or attain saturated shape and dimensions and propagate in a self-similar manner through the material, as, for example, in a CT sample [8]. Intact fibres bridging the macro-crack may fail due to surface flaws [10] at any position along their crack-exposed

lengths or along their length inside the matrix, mainly across the debonding length. Due to the regularly weak nature of the interface, the debond length on the onset of fibre failure is usually much larger than the fibre's crack-exposed length equal to the instant crack opening displacement. Consequently, the probability of a fibre failing along the debond length is much larger than that of a fibre failing within the crack flanks [14]. The same concept can be used to rationalize the fact that strong interfaces are generally undesirable in CFCCs, as the resultant strong bonding between fibres and the matrix promotes fibre fracture without debonding and supports material brittleness instead of decreasing it. Besides its statistical origin, this "preferable fibre failure location" phenomenon is additionally promoted by sliding of the stretching intact fibre's surface across the debonded interface, an action that triggers fibre failure by tampering with the fatal nature of its surface flaws. Fibres failing along the debond length contribute to the pull-out mechanism where shear forces develop between the matrix and fibres due to frictional sliding of the failed fibre's surface across the interface. On the onset of total fibre failure, the composite's behaviour is controlled purely by the pull-out mechanism that endures until all fibres have pulled out completely, disengaging from the matrix.

2.2. Matrix contribution

A mechanically loaded monolithic ceramic will fail in a brittle manner, exhibiting minimal deviation from the linear elastic behaviour up to catastrophic failure. On the other hand, the ceramic matrix of a CFCC will fail gradually and in a stepwise manner due to normally existing open and closed porosity, the interactions with the fibres and the interface. Crack deflection along the interface, interfacial debonding and stepwise multi-failure of matrix parts between fibres and fibre bundles are damage mechanisms that contribute to the ductility of the matrix fracture behaviour. This gradual failure can be approximated by a Weibull distribution function where the load–displacement contribution of the matrix is expressed by:

$$P_m(d) = \frac{1}{C_{m,0}} \cdot d \cdot \exp\left[-\left(\frac{d}{d_{m,0}}\right)^{m_m}\right] \tag{1}$$

where $P_m(d)$ is the load carried by the matrix as a function of displacement d, $C_{m,0}$ is the elastic compliance of the matrix and m_m and $d_{m,0}$ are the respective Weibull shape and location parameters of the matrix. The compliance $C_{m,0}$ is related to the matrix properties through:

$$C_{m,0} = \frac{L}{A_{comp}(1 - V_f)E_m} \tag{2}$$

where L is the reference length over which displacement is measured, A_{comp} is the cross-sectional area of the composite, V_f is the fibre volume fraction and E_m is the Young's modulus of the matrix. By substituting Eq. (1) in Eq. (2) the following expression is obtained:

$$P_m(d) = \frac{A_{comp}(1 - V_f)E_m}{L} \cdot d \cdot \exp\left[-\left(\frac{d}{d_{m,0}}\right)^{m_m}\right] \tag{3}$$

2.3. Intact/bridging fibres contribution

The two-parameter Weibull model is commonly established as the most suitable fibre failure distribution function as it couples a first-order growth term with an exponential decay term that can realistically simulate the sequential phenomena of elastic deformation and incremental fibre failure under the global load-sharing principle, respectively [10,15]. Analogously to Eq. (3), the intact fibre's contribution to the load–displacement behaviour of the composite can be expressed as:

$$P_f(d) = \frac{A_{comp}V_fE_f}{L} \cdot d \cdot \exp\left[-\left(\frac{d}{d_{f,0}}\right)^{m_f}\right] \tag{4}$$

where E_f is the Young's modulus of the fibres and m_f and $d_{f,0}$ their Weibull shape and location parameters.

2.4. Pull-out contribution

Contrary to the intact/bridging fibres contribution to the load–displacement behaviour of a composite, which is associated with axial forces, the origins of the pull-out mechanism are shear forces developing along the debonded interface. The shear force acting on a single fibre on the onset of pull-out can be converted to axial force $T_f(l_p)$ by taking a simple force balance around the fibre:

$$T_f(l_p) = (2\pi r_f \cdot l_p) \cdot \tau \tag{5}$$

where l_p is the pull-out length, τ is the interfacial shear stress and r_f is the fibre radius. The pull-out length is a statistical parameter that may vary among fibres in the composite. Although the exact pull-out length distribution of a composite may be measured post mortem directly on the composite, for the scope of this analysis, and without loss of generality, the mean pull-out length $\overline{l}_p$ can be used in Eq. (5).

The number of failed fibres at any instance during composite fracture, N_p, is reciprocal to the number of surviving (bridging) fibres in the composite. Hence

$$N_p = N_0 \cdot [1 - p_s(d)] \tag{6}$$

where N_0 is the total number of fibres in the composite. $p_s(d)$ is the survival probability of a fibre at a displacement d and is given by:

$$p_s(d) = \exp\left[-\left(\frac{d}{d_{f,0}}\right)^{m_f}\right] \tag{7}$$

However, among the total number of failed fibres, only those that are oriented non-perpendicularly to the loading direction can contribute to pull-out. Denoting by $N_{0,eff}$ the portion of the total number of fibres in the composite that are pull-out-effective, and by combination of Eqs. (6) and (7), the effective number of pull-out fibres is obtained as:

$$N_{\text{p,eff}} = N_{0,\text{eff}} \cdot \left\{ 1 - \exp\left[-\left(\frac{d}{d_{\text{f},0}} \right)^{m_{\text{f}}} \right] \right\} \qquad (8)$$

$N_{0,\text{eff}}$ can be evaluated through the pull-out-effective volume of the composite given by:

$$N_{0,\text{eff}} = \frac{A_{\text{comp}} V_{\text{f,eff}}}{\pi r_{\text{f}}^2} \qquad (9)$$

where $V_{\text{f,eff}}$ is the pull-out-effective fibre volume fraction of the composite.

The force exerted on the composite at the onset of total fibre failure, T, can be expressed as the product of Eqs. (5) and (9):

$$T = \frac{2 A_{\text{comp}} V_{\text{f,eff}} \overline{l_{\text{p}}} \tau}{r_{\text{f}}} \cdot \left\{ 1 - \exp\left[-\left(\frac{d}{d_{\text{f},0}} \right)^{m_{\text{f}}} \right] \right\} \qquad (10)$$

Table 1
Designation of regression parameters

Parameter	Status	Value/reference
Macroscopical parameters		
Gauge length, L	F	25 mm
Cross-sectional area, A_{comp}	F	Specimen-dependent
Material properties		
Young's modulus of matrix, E_{m}	UV	
Young's modulus of fibres, E_{f}	UV	
Fibre radius, r_{f}	F	7 μm [16,17]
Fibre volume fraction, V_{f}	F	0.35 [18]
Weibull parameters		
Weibull modulus of matrix, m_{m}	UV	
Weibull modulus of fibres, m_{f}	UV	
Characteristic failure displacement of matrix, $d_{\text{m},0}$	UV	
Characteristic failure displacement of fibres, $d_{\text{f},0}$	UV	
Displacement at first fibre failure, d_{f}^*	CV (see Table 2)	
Interface-related parameters		
Interfacial shear stress, τ	UV	
Mean pull-out length, $\overline{l_{\text{p}}}$	F in $\overline{l_{\text{p}}} \tau / r_{\text{f}}$	690 mm [16]
	UV in $\exp[-(d - d_{\text{f}}^*)/\overline{l_{\text{p}}}]$	

F: Fixed, UV: unconditionally varying, CV: conditionally varying.

Table 2
Initial and boundary conditions of the regression procedure

	Condition	Origin/rationalization
	Initial conditions	Origin
	Material properties	
IC.1	$E_{\text{m}} = 80$ GPa	Approximate engineering value for glass
IC.2	$E_{\text{f}} = 260$ GPa	Approximate engineering value for ceramic fibre
	Weibull parameters	
IC.3	$m_{\text{m}} = 10$	Approximate engineering value for brittle failure
IC.4	$m_{\text{f}} = 6$	Approximate engineering value for ceramic fibre
IC.5	$d_{\text{m},0} = 0.05$ mm	Experimental load–displacement behaviour
IC.6	$d_{\text{f},0} = 0.15$ mm	Experimental load–displacement behaviour
IC.7	$d_{\text{f}}^* = 0.02$ mm	Experimental load–displacement behaviour
	Interface-related parameters	
IC.8	$\tau = 5$ MPa	Approximate engineering value for moderate bonding
	Boundary conditions	*Rationalization*
BC.1	The matrix contribution term, Eq. (3), may not extend to displacements larger than the value corresponding to the maximum load	Typical brittle fracture. Optical microscope observation that macro-crack and corresponding bridging zone are fully developed, spanning the width of the notched ligament, before the maximum load is attained [13]
BC.2	The intact fibres contribution term, Eq. (4), may not extend to displacements corresponding to pure pull-out	Eq. (16) does not intrinsically relate the confined ranges of effect of intact and failed fibre distribution
BC.3	The value of d_{f}^* is defined by the displacement where the intact fibre contribution term deviates from linearity	Eq. (16) does not intrinsically relate first fibre failure to appearance of pull-out

As the composite displaces further, failed fibres gradually disengage from the matrix and the pull-out length, over which shear forces are acting, decreases. This effect leads to a decrease, with increasing displacement, in the axial force exerted to the composite due to pull-out. It has been shown that the decrease in load due to pull-out of failed fibres follows a first-order exponential decay function, with the decay constant being equal to the mean pull-out length, $\overline{l}_p$ [10].

Based on the above, the total pull-out force as a function of specimen displacement, $T_{tot}(d)$, can be written as:

$$T_{tot}(d) = \frac{2A_{comp}V_{f,eff}\overline{l}_p\tau}{r_f} \cdot \left\{ 1 - \exp\left[-\left(\frac{d}{d_{f,0}} \right)^{m_f} \right] \right\}$$
$$\cdot \exp\left(-\frac{d}{\overline{l}_p} \right) \qquad (11)$$

Eq. (11) generates non-zero values even for infinitesimally small displacements. However, in practice, the appearance of the pull-out mechanism is triggered by the first fibre failure, an action occurring after the end of the fibres' elastic displacement regime. In order to account for this effect, the total pull-out force Eq. (11) can be shifted in displacement by the displacement at which the intact/bridging fibre failure distribution Eq. (4) deviates from linearity, denoted by d_f^*. This leads to:

$$T_{tot} = \frac{2A_{comp}V_{f,eff}\overline{l}_p\tau}{r_f} \cdot \left\{ 1 - \exp\left[-\left(\frac{d - d_f^*}{d_{f,0}} \right)^{m_f} \right] \right\}$$
$$\cdot \exp\left[-\frac{d - d_f^*}{\overline{l}_p} \right] \qquad (12)$$

2.5. Total modelled behaviour

The theoretically expected load–displacement behaviour of the composite can be expressed as the sum of Eqs. (3), (4) and (12):

$$P_{comp}(d) = P_m(d) + P_f(d) + T_{tot}$$
$$= \frac{A_{comp}}{L} \cdot d$$
$$\cdot \left(\begin{array}{l} (1 - V_f)E_m \cdot \exp\left[-\left(\frac{d}{d_{m,0}} \right)^{m_m} \right] + V_f E_f \cdot \exp\left[-\left(\frac{d}{d_{f,0}} \right)^{m_f} \right] + \\ + \frac{2}{d}\frac{\overline{l}_p V_{f,eff}\tau}{r_f}\left\{ 1 - \exp\left[-\left(\frac{d - d_f^*}{d_{f,0}} \right)^{m_f} \right] \right\} \cdot \exp\left[-\frac{d - d_f^*}{\overline{l}_p} \right] \end{array} \right)$$
$$(13)$$

As demonstrated through Eq. (13), the modelled fracture behaviour of the composite depends on:

- macroscopical parameters such as specimen cross-sectional area A_{comp} and the gauge length over which displacement is measured, L;
- the properties of the matrix (such as E_m), of the fibres (such as E_f and r_f) and of the composite (such as the total and effective fibre volume fractions, V_f and $V_{f,eff}$, respectively);
- statistical parameters describing the characteristic failure displacements $d_{m,0}$, $d_{f,0}$ and shape of the Weibull distributions m_m, $m_{m,f}$ for the matrix and fibres, respectively; and
- micromechanical parameters associated with the interface, such as the mean pull-out length, $\overline{l}_p$ and the interfacial shear stress, τ.

In displacement-controlled testing, the total displacement of the material is the sum of a linear contribution

Table 3
Results of the regressions

Specimen constants	Value		
	Specimen 1	Specimen 2	Specimen 3
Specimen width, W (mm)	12	12	10
Specimen thickness, t (mm)	2	2	3
Notch-to-width ratio, $2\alpha_0/W$ (–)	0.6	0.4	0.4
Cross-section area, $A_{comp} = tW(1 - 2a_0/W)$ (mm^2)	9.6	14.4	18
Varying parameters	Regression output values		
Material properties			
Young's modulus of matrix, E_m (GPa)	73.9	63.2	71.5
Young's modulus of fibres, E_f (GPa)	221.0	189.0	213.8
Weibull parameters			
Weibull modulus of matrix, m_m (–)	1.885	1.895	1.889
Weibull modulus of fibres, m_f (–)	2.540	2.525	2.520
Char. failure displacement of matrix, $d_{m,0}$ (mm)	0.0357	0.0351	0.0390
Char. failure displacement of fibres, $d_{f,0}$ (mm)	0.0915	0.1040	0.0901
Displacement at first fibre failure, d_f^* (mm)	0.0197	0.0190	0.0190
Interface-related parameters			
Interfacial shear stress, τ (MPa)	2.86	3.04	3.21
Mean pull-out length, $\overline{l}_p$ (mm)	0.506	0.615	0.588
Computed parameters	Value		
Composite elastic modulus (GPa)	125.4	107.2	121.3

corresponding to reversible deformation and a non-linear contribution corresponding to the irreversible mechanism of fracture, which, in turn, is directly associated with crack opening and the corresponding formation of the bridging zone. In simple specimen configurations, such as a double-edge-notched tension specimen, a direct relation can be drawn between the crack opening, e, and the load carried by intact/bridging and failed/pull-out fibres within that crack opening, $P_{br}(e)$, by subtracting the elastic displacement from the total displacement of the system:

$$e(d) = d - C_0 P_{comp}(d) \qquad (14)$$

where C_0 is the compliance of the composite within the elastic regime. $P_{br}(e)$ can then be expressed as the sum of Eqs. (3) and (4) considered with respect to e, while the bridging law, $\sigma_{br}(e)$, can be obtained by dividing $P_{br}(e)$ by the cross-sectional area of the composite, A_{comp}. The above leads to:

$$\sigma_{br}(e) = \frac{V_{f,eff}}{L} \cdot d \cdot \left(E_f \cdot \exp\left[-\left(\frac{e}{e_{f,0}} \right)^{m_f} \right] \right.$$
$$\left. + \frac{2}{d} \frac{\overline{l_p} \tau}{r_f} \left\{ 1 - \exp\left[-\left(\frac{e - e_f^*}{e_{f,0}} \right)^{m_f} \right] \right\} \cdot \exp\left[-\frac{e - e_f^*}{\overline{l_p}} \right] \right) \qquad (15)$$

It is important to note that only fibres that are oriented non-perpendicularly to the loading direction can contribute to bridging. Hence, only the effective fibre volume fraction $V_{f,eff}$ is relevant for the intact-fibre term of the bridging law. In the present case, the model is applied in a cross-ply laminate for the fibers that are parallel to the loading direction, hence the calculation of $V_{f,eff}$ is trivial. In case of existing other reinforcing directions, $V_{f,eff}$ must be calculated before application of the model.
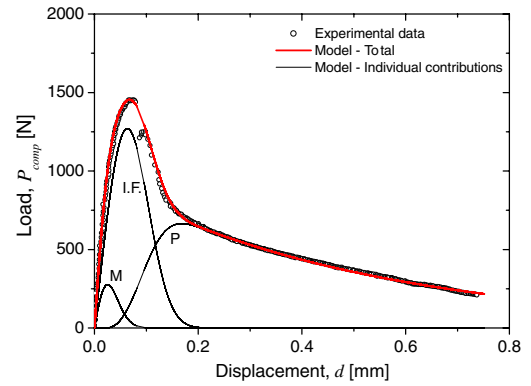
3. Application to composite

The established model, Eq. (13), was validated against the experimentally recorded load–displacement behaviour of DEN SiC-fibre-reinforced glass–ceramic matrix composite coupons tested under uniaxial monotonic tension. For the $[0/90]_{ns}$ (where $n = 2$ and 3) cross-ply laminate used in this study, the effective fibre volume fraction is given as $V_{f,eff} = V_f/2$ and Eq. (13) attains the form:
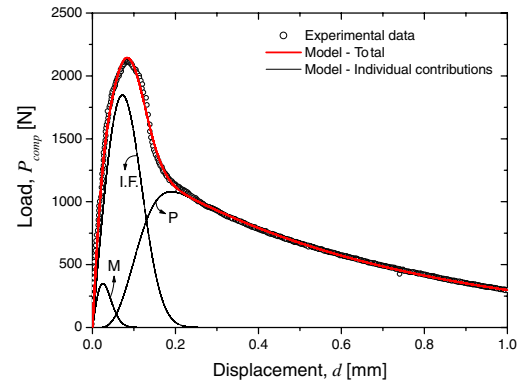
$$P_{comp}(d) = \frac{A_{comp} V_f}{L} \cdot d$$
$$\cdot \left(\begin{array}{c} \frac{(1-V_f)E_m}{V_f} \cdot \exp\left[-\left(\frac{d}{d_{m,0}} \right)^{m_m} \right] + E_f \cdot \exp\left[-\left(\frac{d}{d_{f,0}} \right)^{m_f} \right] + \\ + \frac{1}{d} \frac{\overline{l_p} \tau}{r_f} \left\{ 1 - \exp\left[-\left(\frac{d - d_f^*}{d_{f,0}} \right)^{m_f} \right] \right\} \cdot \exp\left[-\frac{d - d_f^*}{\overline{l_p}} \right] \end{array} \right) \qquad (16)$$

The assessment of the original $P_{comp}(d)$ behaviour of the composite was performed computationally through an iterative regression procedure where convergence was controlled by the x^2 reduction criterion (computed for the total fit).
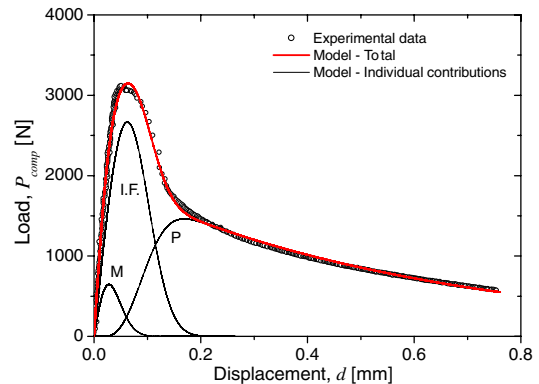
Given the large number of parameters utilized in Eq. (16), an infinite number of combinations of their values can leave the expression invariant. In this regard, experimental values were introduced for parameters entering as multipliers or divisors in the same terms. Care was taken in introducing only those parameters that are easily measurable while keeping the number of introduced constants to an absolute minimum. In this rationale, unambiguously determinable material properties such as elastic and Weibull moduli were free to vary during the regression proce-

a. Specimen 1 (t=2.0 mm, W=12 mm, $2\alpha_0/W$=0.6)

b. Specimen 2 (t=12.0 mm, W=12 mm, $2\alpha_0/W$=0.4)

c. Specimen 3 (t=3.0 mm, W=10 mm, $2\alpha_0/W$=0.4)

Fig. 1. Assessment of the experimentally obtained load–displacement behaviour of the composite by the established model. The individual contributions of matrix, intact/bridging and failed/pull-out fibres are denoted by indices M, I.F. and P respectively.

dure in order for their output values to serve in validating the efficiency of the performed regression. Fibre radius, r_f, and experimental constants such as specimen cross-sectional area, A_{comp}, and the gauge length of the extensometer used for recording displacement on the specimen, L, were introduced per se. By examination of Eq. (16) it is observed that the fibre volume fraction, V_f, and one of $\overline{l_p}$ or τ must also be fixed. Although reference values for the interfacial shear stress of the specific composite exist [16], it was chosen that $\overline{l_p}$ be fixed and τ be deduced due to the simplicity associated with the experimental measurement of pull-out length as opposed to the difficulties encountered in measuring interfacial shear stress. The validity of this remark is supported by the large spread of values for τ available in the literature, ranging, for the specific composite, between 2 and 5 MPa (relevant coefficient of variation 60%), in contrast to the unambiguous measurements of mean pull-out length, $\overline{l_p}$, with values ranging between 670 and 710 μm (relevant coefficient of variation 2%) [16]. As will be demonstrated in a later section of this study, a variation in the value of τ by 2 MPa (approximately equal to only half the standard deviation from the mean of 3.5 MPa within the 2–5 MPa range) has a dramatic effect on the load–displacement behaviour of the composite. On the other hand, a variation in $\overline{l_p}$ by 30 μm (equal to twice the standard deviation from the mean 690 μm within the 670–710 μm range) has a minor effect. One exception to the above was that the mean pull-out length, $\overline{l_p}$, was chosen to vary in the last exponential term of Eq. (16), $\exp[-(d - d_f^*)/\overline{l_p}]$, when it enters independently. A list of all parameters used in the regression procedure is presented in Table 1.

Common to the aforementioned case, a large number of combinations among the individual contributions of the matrix, intact and failed fibres can leave Eq. (16) invariant. Analogously, the minimum possible number of initial and boundary conditions with respect to the independent variable, d, were introduced in order to realistically relate the range of effect of the individual contributions. These conditions are tabulated in Table 2.

Table 3 lists the results of three regressions performed on the experimental load–displacement behaviours of equal-in-number DEN specimens with different thicknesses and notch-to-width ratios. The regressions are depicted in graphical form in Fig. 1.

As manifested through Fig. 1, as well as through the values of output parameters in Table 3, the model is successful in assessing the actual fracture behaviour of the composite. This remark is supported by the correlation coefficients of the regressions, which did not exceed a value of 0.997 in all cases. The most important finding, though, is the fact that the values of output parameters remain practically constant among specimens of different thickness and notch depths, and hence also of bridging zone dimensions. Table 4 summarizes the statistical properties of the output parameters along with reference values for known quantities. It is observed that parameter values vary within 10% among specimens of different dimensions. Considering the role of interfacial shear stress, the accuracy associated with the determination of this parameter as compared with its wide spread in the literature is of particular importance. Equally important is the value obtained for the fibres' Weibull modulus that, although initially set to a much higher value (IC.4, Table 2), exhibits smaller scatter from the mean output value of 2.5 that compares favourably with the reference.

The modelled bridging law and the corresponding individual contributions of intact and pull-out fibres can be calculated for each specimen through Eqs. (14) and (15). At the same time, the crack growth resistance of the material can be obtained by integration of the bridging law with respect to crack opening while the individual contributions of intact and pull-out fibres to the resistance can be obtained as the integrals of the corresponding bridging law terms. The obtained bridging law and R-curves are presented in Fig. 2.

Table 4
Statistical properties of regressions

Varying parameters	Mean, μ	SD, σ	Variance, σ/μ (%)	Reference
Material properties				
Young's modulus of matrix, E_m (GPa)	69.5	5.62	8.08	70 [18]
Young's modulus of fibres, E_f (GPa)	207.9	16.82	8.09	200 [18]
Weibull parameters				
Weibull modulus of matrix, m_m (–)	1.889	0.0047	0.24	–
Weibull modulus of fibres, m_f (–)	2.528	0.0100	0.39	2.3–2.7 [17]
Char. failure displacement of matrix, $d_{m,0}$ (mm)	0.0366	0.00210	5.73	–
Char. failure displacement of fibres, $d_{f,0}$ (mm)	0.0952	0.00768	8.06	–
Displacement at first fibre failure, d_f^* (mm)	0.0193	0.00041	2.12	–
Interface-related parameters				
Interfacial shear stress, τ (MPa)	3.04	0.174	5.72	2–5 [16]
Mean pull-out length, $\overline{l_p}$ (mm)	0.570	0.0569	9.98	0.690 [16]
Extracted parameters				
Composite elastic modulus (GPa)	117.9	9.54	8.09	123 [18]

Specimen 1 (t=12.0 mm, W=12 mm, $2\alpha_0/W$=0.4)

Specimen 2 (t=2.0 mm, W=12 mm, $2\alpha_0/W$=0.6)

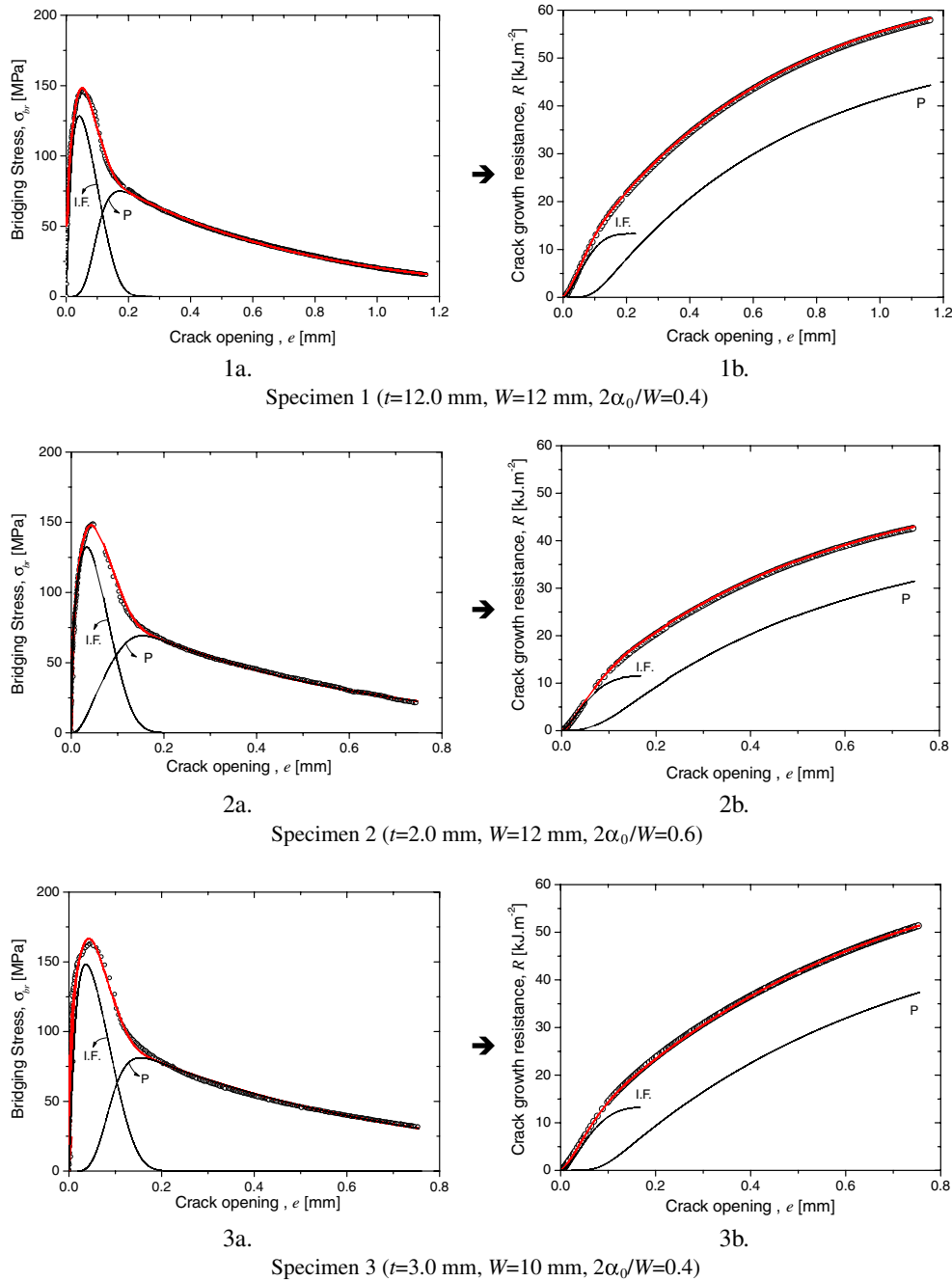Specimen 3 (t=3.0 mm, W=10 mm, $2\alpha_0/W$=0.4)

Fig. 2. Experimental and modelled bridging laws (left column) and R-curves (right column).

4. Discussion

The agreement between analytical and experimental findings, as well as the accordance with the values of calculated parameters in the literature, is representative of the potential of the model to assess the fracture behaviour of the specific composite system in a realistic manner. On the other hand, the ability of the model to predict, a priori, the macromechanical fracture behaviour of any given composite (load–displacement behaviour, bridging law and R-curve) can be limited by the lack of knowledge of certain parameters' values. However, all parameters

used in the model have explicit physical meaning and are experimentally measurable quantities. It is also understood that use of the specific model expression is valid only for simple geometries where fracture is not confined by specimen configuration characteristics, such as in a three-point bending or in a compact tension specimen. In fact, in such cases the established law can be utilized once modified to account for the specific needs of the geometry [14]. Nevertheless, an analysis of the effect of selected parameters on the magnitude and shape of load–displacement behaviour, bridging law and R-curve of the material under the current configuration is of particular interest.

The effect of fibre volume fraction, Weibull modulus of fibres and interfacial shear stress on three fracture descriptors are presented in Fig. 3(1), (2) and (3), respectively. The values of varying parameters are included in the corresponding graph legends while the values of the remaining parameters were in every case kept constant to the mean values obtained through the regression procedure (Table 4).

The effect of fibre volume fraction in the fracture behaviour of the composite is presented in Fig. 3(1) (left column graphs). It is observed that lower values of V_f result in a decrease in the maximum load attainable by the composite while, at the same time, causing a decrease in the pull-out contribution to the crack resistance of the material. This dual role of fibre volume fraction stems from the ability of the fibres to serve both as reinforcing media in the intact state and as surface area providers for the development of frictional forces in the failed state. By examination of Fig. 3(1), a vast change in the crack growth resistance capacity of the material is observed for a shift in volume fraction by 17% while the specific parameter comes into effect, as expected, only after the first matrix crack occurs.

The effect of fibre Weibull modulus on the total fracture behaviour of the composite follows a more complex scenario. Fig. 3(2a) manifests that fibres of higher Weibull modulus contribute to the attainment of higher maximum loads. However, the sharper decrease in the intact fibre contribution associated with higher Weibull modulus indicates a more massive, hence also more critical, composite failure scenario. The effect of Weibull modulus on load vanishes after the composite fracture changes to being purely pull-out-dominated. It is interesting to note that,
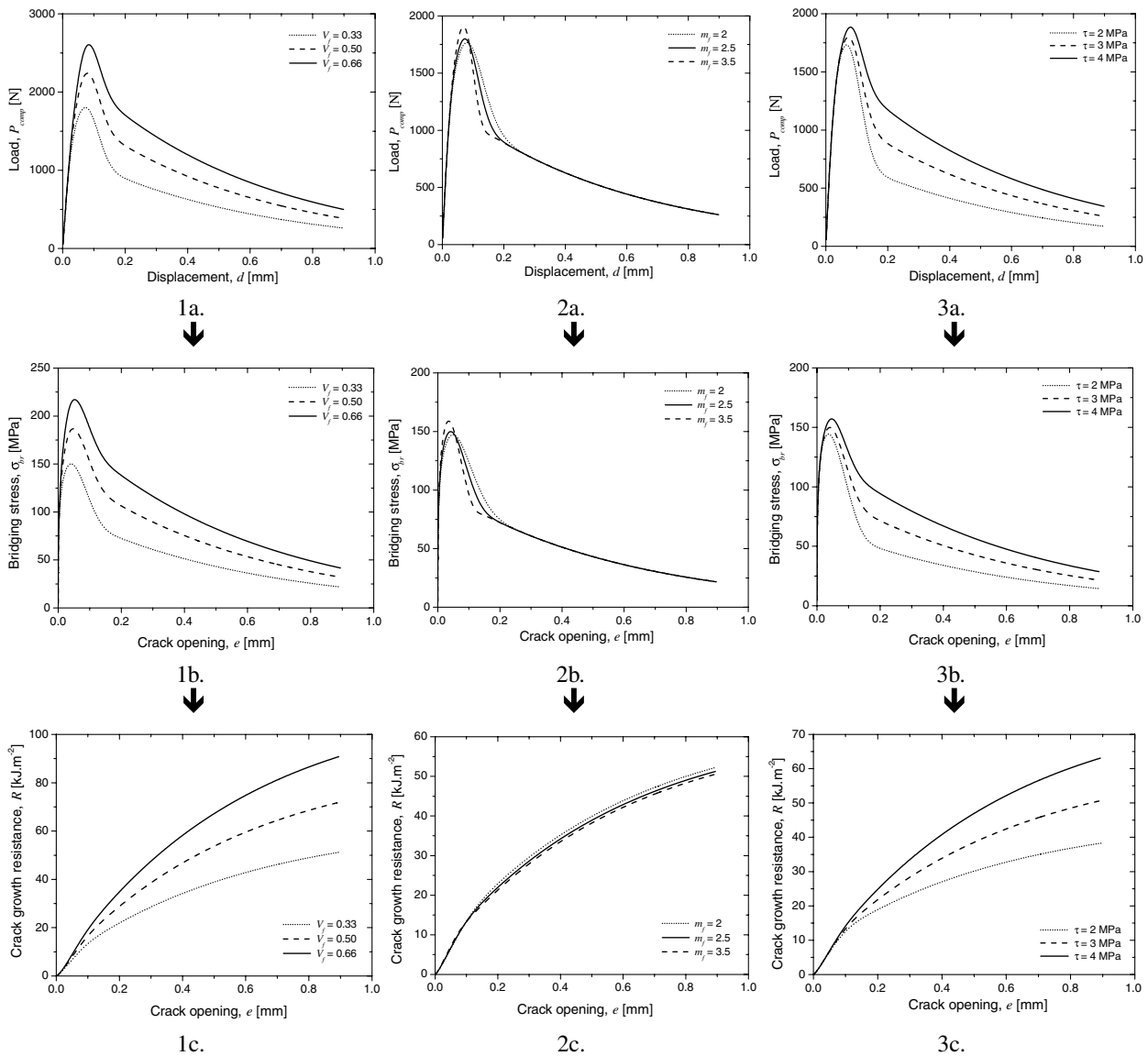

Fig. 3. Effect of fibre volume fraction (1), Weibull modulus of fibres (2) and interfacial shear stress (3) on load–displacement behaviour of the composite (a), bridging law (b) and crack growth resistance (c).

while the effect of Weibull modulus is clear in the load–displacement curve within the fibre failure regime, the same does not hold for the R-curve, where a limited shift in crack growth resistance is noted at displacements corresponding to pure pull-out. The observed shift stems from the dependence of the characteristic failure displacement upon the Weibull modulus, with higher values of the latter providing lower values for the former. The same dependence is responsible for the small effect of this parameter within the fibre failure regime of the R-curve: by increasing maximum bridging stress while simultaneously decreasing the width of the intact fibre distribution, a higher Weibull modulus leaves the integral of this contribution practically invariant.

The interfacial shear stress appears to affect most dramatically the mechanical performance of the composite (Fig. 3(3)). The role of τ, as demonstrated through Eq. (12), is analogous to that of the fibre volume fraction with the exception that the former comes into effect after first fibre failure. Higher values of this parameter induce the development of more intense shear – hence also axial – forces during frictional sliding of the intact or failed fibres surface along the debonded interface. It is of particular interest to observe that, for the range of bibliographically available values of τ for the composite of this study, 2–5 MPa, all three fracture descriptors, load–displacement, bridging law and R-curve, change radically.

In this regard, the ability of the established model to predict a priori the fracture behaviour of a specific CFCC exhibiting LSB relies catalytically on the precision of the introduced value for interfacial shear stress which, common to all parameters entering the model, is an experimentally measurable quantity of explicit physical significance. It is still interesting to note, however, that the same parameters can also be evaluated through the assessment of the experimental load–displacement behaviour of a single test specimen by the law proposed in this study, Eq. (13).

5. Conclusions

A bridging law model has been developed for the assessment of the fracture behaviour of continuous-fibre-reinforced ceramic matrix composites based on composite parameters, as well as on micromechanical properties of fibres, matrix and the interface. The model formulation relies on the concept of convolution of the load–displacement behaviour of the composite into the individual, appropriately coupled contributions of matrix, intact/bridging and failed/pull-out fibres. The established law assesses the load–displacement behaviour while a simple concept equating the non-linear part of displacement to crack opening is used to convert the original form into bridging law and, in turn, into crack growth resistance of the material. The law was successful in assessing the experimentally established load–displacement behaviour of a notched SiC-fibre-reinforced ceramic matrix composite with LSB characteristics tested in monotonic tension. The output values of the regression parameters remained practically constant among specimens of varying cross-sectional areas and notch lengths. The model was utilized in analysing the effect of selected parameters in composite performance, as well as in linking the micromechanical interactions with the macroscopic response of the material to applied deformation.

References

[1] Cox BN. Acta Mater 1991;39:1189.
[2] Fett T, Munz D, Geraghty RD, White KW. Eng Fract Mech 2000;66:375.
[3] Foote RML, Mai Y-W, Cotterell B. J Mech Phys Solids 1986;34:593.
[4] Rausch G, Kuntz M, Gratwohl G. J Am Ceram Soc 2000;84:2762.
[5] Sorensen BF, Jacobsen TK. Compos Part A-Appl S 1998;29:1443.
[6] Jacobsen TK, Sorensen BF. Compos Part A-Appl S 2001;32:1.
[7] Hu XZ, Mai YW. J Mater Sci 1992;27:3502.
[8] Pappas YZ, Kostopoulos V. Eng Fract Mech 2001;68:1557.
[9] Fett T, Munz D. J Eur Ceram Soc 1995;15:337.
[10] Sutcu M. Acta Mater 1989;37:651.
[11] Thouless MD, Evans AG. Acta Metall 1988;36:517.
[12] Llorca J, Singh N. J Am Ceram Soc 1991;74:2882.
[13] Dassios KG, Galiotis C, Kostopoulos V, Steen M. Acta Mater 2003;51:5359.
[14] Dassios KG, PhD thesis. Department of Mechanical Engineering and Aeronautics, University of Patras, Greece, 2003.
[15] Dassios KG, Steen M, Filiou K. Mat Sci Eng A Struct 2003;349:63.
[16] Brenet P, Concin F, Fantozzi G, Reynaud P, Rouby D, Tallaron C. Compos Sci Technol 1996;56:817.
[17] Simon G, Bunsell AR. J Mater Sci 1984;19:3649.
[18] Drissi-Habti M. J Eur Ceramic Soc 1997;17:33.